

The dynamics of starvation and recovery

2 Justin D. Yeakel * †‡, Christopher P. Kempes †, and Sidney Redner †§

3 *School of Natural Science, University of California Merced, Merced, CA, †The Santa Fe Institute, Santa Fe, NM, §Department of Physics, Boston University, Boston
4 MA, and ‡To whom correspondence should be addressed: jdyeakel@gmail.com

5 Submitted to Proceedings of the National Academy of Sciences of the United States of America

6 The eco-evolutionary dynamics of species is fundamentally linked
7 to the energetic constraints of individuals. Of particular impor-
8 tance are the tradeoffs between reproduction and the dynamics
9 of starvation and recovery in resource limited environments. We
10 introduce a minimal nutritional state-structured model that in-
11 corporates two classes of consumer: nutritionally replete con-
12 sumers that reproduce, and undernourished, non-reproducing
13 consumers that are susceptible to mortality. As a function of the
14 energetic rates between these replete and undernourished states
15 that are determined by the presence or absence of resources,
16 the consumer populations can either undergo cyclic dynamics or
17 reach a steady state. We obtain strong constraints on starvation
18 and recovery rates by deriving allometric scaling relationships
19 and find that population dynamics subject to these constraints
20 can approach the cyclic regime but are typically driven to a steady
21 state. Moreover, we find these rates fall within a ‘refuge’ in pa-
22 rameter space, where the probability of extinction of the consumer
23 population is minimized. Thus we introduce a potential mech-
24 aism that may both drive and constrain the dynamics of animal
25 populations. Importantly, our model provides a natural framework
26 that predicts maximum body size for mammals by examining the
27 relative stability of an otherwise homogeneous population to a
28 mutant population with altered percent body fat. For body masses
29 $\lesssim 10^6$ g, an invader with increased percent body fat dominates over
30 the resident population, and vice versa for body mass $\gtrsim 10^6$ g,
31 thus providing a principled mechanism for a within-lineage driver
32 of Cope’s rule.

33 foraging | starvation | reproduction

34 Introduction

35 The behavioral ecology of most, if not all, organisms is influ-
36 enced by the energetic state of individuals, which directly influ-
37 ences how they invest reserves in uncertain environments. Such
38 behaviors are generally manifested as trade-offs between invest-
39 ing in somatic maintenance and growth, or allocating energy
40 towards reproduction [1, 2, 3]. The timing of these behaviors
41 responds to selective pressure, as the choice of the investment
42 impacts future fitness [4]. The influence of resource limitation
43 on an organism’s ability to maintain its nutritional stores may
44 lead to repeated delays or shifts in reproduction over the course
45 of an organism’s life.

46 The balance between (a) somatic growth and maintenance,
47 and (b) reproduction is often conditioned on resource availabil-
48 ity [5]. For example, reindeer invest less in calves born after
49 harsh winters (when the mother’s energetic state is depleted)
50 than in calves born after moderate winters [6]. Many bird
51 species invest differently in broods during periods of resource
52 scarcity compared to normal periods [7, 8], sometimes delaying
53 or even foregoing reproduction for a breeding season [1, 9, 10].
54 Even freshwater and marine zooplankton have been observed to
55 avoid reproduction under nutritional stress [11], and those that
56 do reproduce have lower survival rates [2]. Organisms may also
57 separate maintenance and growth from reproduction over space
58 and time: many salmonids, birds, and some mammals return to
59 migratory breeding grounds to reproduce after one or multiple
60 seasons in resource-rich environments where they accumulate
61 nutritional reserves [12, 13, 14].

62 Physiological mechanisms also play an important role in
63 regulating reproductive expenditures during periods of resource
64 limitation. The data collected thus far has shown that diverse

65 mammals (47 species in 10 families) exhibit delayed implan-
66 tation, whereby females postpone fetal development (blasto-
67 cyst implantation) until nutritional reserves can be accumu-
68 lated [15, 16]. Many other many species (including humans)
69 suffer irregular menstrual cycling and higher spontaneous abor-
70 tion rates during periods of nutritional stress [17, 18]. In the
71 extreme case of unicellular organisms, nutrition is unavoidably
72 linked to reproduction because the nutritional state of the cell
73 regulates all aspects of the cell cycle [19]. The existence of so
74 many independently evolved mechanisms across such a diverse
75 suite of organisms highlights the importance and universality
76 of the fundamental tradeoff between somatic and reproductive
77 investment. However the dynamic implications of these con-
78 straints are unknown.

79 Though straightforward conceptually, incorporating the en-
80 ergetic dynamics of individuals [20] into a population-level
81 framework [20, 21] presents numerous mathematical obsta-
82 cles [22]. An alternative approach involves modeling the
83 macroscale relations that guide somatic versus reproductive
84 investment in a consumer-resource system. For example,
85 macroscale Lotka-Volterra models assume that the growth rate
86 of the consumer population depends on resource density, thus
87 implicitly incorporating the requirement of resource availability
88 for reproduction [23].

89 In this work, we adopt an alternative approach in which
90 resource limitation and the subsequent effect of starvation is
91 accounted for explicitly. Namely, only individuals with suffi-
92 cient energetic reserves can reproduce. Such a constraint leads
93 to reproductive time lags due to some members of the pop-
94 ulation going hungry and then recovering. Additionally, we
95 incorporate the idea that reproduction is strongly constrained
96 allometrically [3], and is not generally linearly related to re-
97 source density. As we shall show, these constraints influence
98 the ensuing population dynamics in dramatic ways.

99 Nutritional state-structured model (NSM)

100 We begin by defining a minimal Nutritional State-structured
101 population Model (NSM), where the consumer population is
102 divided into two energetic states: (a) an energetically replete
103 (full) state F , where the consumer reproduces at a constant
104 rate λ and does not die from starvation, and (b) an energeti-
105 cally deficient (hungry) state H , where the consumer does not
106 reproduce but dies by starvation at rate μ . The underlying
107 resource R evolves by logistic growth with an intrinsic growth
108 rate α and a carrying capacity equal to one. Consumers tran-

109 Reserved for Publication Footnotes

sition from the full state F to the hungry state H at a rate σ —the starvation rate—and also in proportion to the absence of resources ($1 - R$). Conversely, consumers recover from state H to state F at rate ρ and in proportion to R . Resources are also eaten by the consumers—at rate ρ by hungry consumers and at rate $\beta < \rho$ by full consumers. This inequality accounts for hungry consumers requiring more resources to replace lost body tissue.

In the mean-field approximation, in which the consumers and resources are perfectly mixed, their densities evolve according to the rate equations

$$\begin{aligned}\dot{F} &= \lambda F + \rho RH - \sigma(1 - R)F, \\ \dot{H} &= \sigma(1 - R)F - \rho RH - \mu H, \\ \dot{R} &= \alpha R(1 - R) - R(\rho H + \beta F).\end{aligned}$$

Notice that the total consumer density $F + H$ evolves according to $\dot{F} + \dot{H} = \lambda F - \mu H$. This resembles the equation of motion for the predator density in the classic Lotka-Volterra model, except that the resource density does not appear in the growth term. As discussed above, the attributes of reproduction and mortality have been explicitly apportioned to the full and hungry consumers, respectively, so that the growth in the total density is decoupled from the resource density.

Equation [1] has three fixed points: two trivial fixed points at $(F^*, H^*, R^*) = (0, 0, 0)$ and $(0, 0, 1)$, and one non-trivial, internal fixed point at

$$\begin{aligned}F^* &= \frac{\alpha\lambda\mu(\mu + \rho)}{(\lambda\rho + \mu\sigma)(\lambda\rho + \mu\beta)}, \\ H^* &= \frac{\alpha\lambda^2(\mu + \rho)}{(\lambda\rho + \mu\sigma)(\lambda\rho + \mu\beta)}, \\ R^* &= \frac{\mu(\sigma - \lambda)}{\lambda\rho + \mu\sigma}.\end{aligned}$$

The stability of this fixed point is determined by the Jacobian Matrix \mathbf{J} , where each matrix element J_{ij} equals $\partial\dot{X}_i/\partial X_j$ when evaluated at the internal fixed point, and \mathbf{X} is the vector (F, H, R) . The parameters in Eq. [1] are such that the real part of the largest eigenvalue of \mathbf{J} is negative, so that the system is stable with respect to small perturbations from the fixed point. Because this fixed point is unique, it is the global attractor for all population trajectories for any initial condition where the resource and consumer densities are both non zero.

From Eq. [2], an obvious constraint on the NSM is that the reproduction rate λ must be less than the starvation rate σ , so that R^* is positive. In fact, when the resource density $R = 0$, the rate equation for F gives exponential growth of F for $\lambda > \sigma$. The condition $\sigma = \lambda$ represents a transcritical (TC) bifurcation that demarcates the physical and unphysical regimes. The biological implication of the constraint $\lambda < \sigma$ has a simple interpretation—the rate at which a macroscopic organism loses mass due to lack of resources is generally much faster than the rate of reproduction. As we will discuss below, this inequality is a natural consequence of allometric constraints [3] for organisms within empirically observed body size ranges (Fig. 2).

In the physical regime of $\lambda < \sigma$, the fixed point [2] may either be a stable node or a limit cycle (Fig. 3). In continuous-time systems, a limit cycle arises when a pair of complex conjugate eigenvalues crosses the imaginary axis to attain positive real parts [24]. This Hopf bifurcation is defined by $\text{Det}(\mathbf{S}) = 0$, with \mathbf{S} the Sylvester matrix, which is composed of the coefficients of the characteristic polynomial of the Jacobian matrix [25]. As the system parameters are tuned to be within the stable regime but close to the Hopf bifurcation, the amplitude of the transient but decaying cycles become large. Given that ecological systems are constantly being perturbed [26], the onset of

When the starvation rate $\sigma \gg \lambda$, a substantial fraction of the consumers are driven to the hungry non-reproducing state. Because reproduction is inhibited, there is a low steady-state consumer density and a high steady-state resource density. Whereas the relation between consumer growth rate λ and the starvation rate σ defines an absolute bound of biological feasibility—the TC bifurcation— σ also determines the sensitivity of the consumer population to changes in resource density.

When $\sigma \gg \lambda$, the steady-state population density is small, thereby increasing the risk of stochastic extinction. On the other hand, as σ decreases, the system will ultimately be poised either near the TC or the Hopf bifurcation (Fig. 3). If the recovery rate ρ is sufficiently small, the TC bifurcation is reached and the resource eventually is eliminated. If ρ exceeds a threshold value, cyclic dynamics will develop as the Hopf bifurcation is approached.

Role of allometry

The NSM describes a broad range of dynamics, yet organisms are likely unable to access most of the total parameter space. Here we use allometric scaling relations to constrain the covariation of rates in a principled and biologically meaningful manner.

Allometric scaling relations highlight common constraints and average trends across large ranges in body size and species diversity. Many of these relations can be derived from a small set of assumptions and below we describe a framework to determine the covariation of timescales and rates across the range of mammals for each of the key parameters of our model (cf. [30]). We are thereby able to define the regime of dynamics occupied by the entire class of mammals along with the key differences between the largest and smallest mammals.

Nearly all of the rates described in the NSM are to some extent governed by consumer metabolism, which can be used to describe a variety of organismal features [31]. The scaling relation between an organism's metabolic rate B and its body size at reproductive maturity $m = M$ (where m denotes body sizes during growth and prior to reproductive maturity) is well documented [32] and scales as $B = B_0 M^\eta$, where η is the scaling exponent, generally assumed to vary around 2/3 or 3/4 for metazoans (e.g. [31]), and has taxonomic shifts for unicellular species between $\eta \approx 1$ in eukaryotes and $\eta \approx 1.76$ in bacteria [33, 3]. An organism's metabolic rate is proportional to the cost of tissue maintenance without growth (i.e. at $m = M$) such that $\beta = \xi B$, where ξ is related to the conversion efficiency of resource to consumer tissue (Supporting Information, section XX).

Several efforts have shown how a partitioning of B between growth and maintenance purposes can be used to derive a general equation for the growth trajectories and growth rates of organisms ranging from bacteria to metazoans [34, 35, 36, 37, 3]. More specifically, the cross-species trends in growth rate can be approximated by

$$\lambda = \lambda_0 M^{\eta-1}. \quad [3]$$

This relation is derived from the simple balance condition $B_0 m^\eta = E_m \dot{m} + B_m m$, [34, 35, 36, 37, 3]

where E_m is the energy needed to synthesize a unit of mass, and $\mu = 1/t_\mu$.

B_m is the metabolic rate to support an existing unit of mass, and m is the mass at any point in development. This balance has the general solution [35, 3]

$$m(t) = \left[1 - \left(1 - \frac{b}{a} m_0^{1-\eta} \right) e^{-b(1-\eta)t} \right]^{1/(1-\eta)} \left(\frac{a}{b} \right)^{1/(1-\eta)} \quad [5]$$

where, $a = B_0/E_m$, $b = B_m/E_m$, and m_0 is mass at birth, which we use to define the timescale of recovery from starvation. The rate of recovery $\rho = 1/t_\rho$ requires that an organism accrues sufficient tissue to transition from the hungry to the full state. Since only certain tissues can be digested for energy (for example the brain cannot be degraded to fuel metabolism), we define the rate for starvation, death, and recovery by the timescales required to reach, or return from, specific fractions of the replete-state mass. Here and henceforth, see Supporting Information, sections XX-XX for details on parameterizations. We define $m_{\text{starve}} = \epsilon M$, where $\epsilon < 1$ is the fraction of replete-state mass where reproduction ceases. This fraction will be modified if tissue composition systematically scales with adult mass. For example, making use of the observation that body fat in mammals scales with overall body size according to $M_{\text{fat}} = f_0 M^\gamma$ and assuming that once this mass is fully digested the organism starves, this would imply that $\epsilon = 1 - f_0 M^\gamma / M$. It follows that the recovery timescale, $t_\rho = t_2 - t_1$, is the time it takes to go from $m(t_1) = \epsilon M$ to $m(t_2) = M$, or

$$t_\rho = \frac{\ln \left[1 - \frac{a}{b} (M)^{1-\eta} \right] - \ln \left[1 - \frac{a}{b} (\epsilon M)^{1-\eta} \right]}{(\eta - 1)b}. \quad [6]$$

It should be noted that more complicated ontogenetic models explicitly handle storage [37], whereas this is implicitly covered by the body fat scaling in our framework.

To determine the starvation rate, σ , we are interested in the time required for an organism to go from a mature adult that reproduces at rate λ , to a reduced-mass hungry state where reproduction is impossible. For starving individuals we assume that an organism must meet its maintenance requirements using the digestion of existing mass as the sole energy source. This assumption implies the following simple metabolic balance

$$\dot{m}E'_m = -B_m m \quad [7]$$

where E'_m is the amount of energy stored in a unit of existing body mass which differs from E_m , the energy required to synthesize a unit of biomass [37]. Given the replete mass, M , of an organism, the above energy balance prescribes the mass trajectory of a non-consuming organism:

$$m(t) = M e^{-b't} \quad [8]$$

where $b' = E'_m/B_m$. The time scale for starvation is given by the time it takes this decay to reach ϵM , which is

$$t_\sigma = -b' \ln(\epsilon). \quad [9]$$

The starvation rate is then $\sigma = 1/t_\sigma$, which scales with replete-state mass as $1/\ln(1 - f_0 M^\gamma / M)$. An important feature is that σ does not have a simple scaling dependence on λ (Eq. 3), which is important for the dynamics that we later discuss.

The time to death should follow a similar relation, but defined by a lower fraction of replete-state mass, $m_{\text{death}} = \epsilon' M$. Suppose, for example, that an organism dies once it has digested all fat and muscle tissues, and that muscle tissue scales with body mass according to $M_{\text{musc}} = u_0 M^\zeta$. This gives $\epsilon' = 1 - (f_0 M^\gamma + u_0 M^\zeta) / M$. Muscle mass has been shown to be roughly proportional to body mass [38] in mammals and thus ϵ' is merely ϵ minus a constant. Thus

$$t_\mu = -b' \ln(\epsilon'),$$

Although these rate equations are general, here we focus on parameterizations for terrestrial-bound endotherms, specifically mammals, which range from a minimum of $M \approx 1$ gram (the Etruscan shrew *Suncus etruscus*) to a maximum of $M \approx 10^7$ grams (the late Eocene to early Miocene Indricotheriinae). Investigating other classes of organisms would simply involve altering the metabolic exponents and scalings associate with ϵ . Moreover, we emphasize that our allometric equations describe mean relationships, and do not account for the (sometimes considerable) variance associated with individual species.

Stabilizing effects of allometric constraints

As the allometric derivations of the NSM rate laws reveal, starvation and recovery rates are not independent parameters, and the bifurcation space shown in Fig. 3 is navigated via covarying parameters. Given the parameters of terrestrial endotherms, we find that σ and ρ are constrained to lie within a small window of potential values (Fig. 4) for the known range of body sizes M . We thus find that the dynamics for all mammalian body sizes is confined to the steady-state regime of the NSM and that limit-cycle behavior is precluded. Moreover, for larger M , the distance to the Hopf bifurcation increases, while uncertainty in allometric parameters (20% variation around the mean; Fig. 4) results in little qualitative difference in the distance to the Hopf bifurcation. These results suggest that small mammals are more prone to population oscillations—including both stable limit cycles as well as transient cycles—than mammals with larger body size. Thus our NSM model predicts that population cycles should be less common for larger species and more common for smaller species, particularly in environments where resources are limiting.

Previous studies have used allometric constraints to explain the periodicity of cyclic populations [39, 40, 41], suggesting a period $\propto M^{0.25}$, however this relation seems to hold only for some species [42], and potential drivers range from predator and/or prey lifespan to competitive dynamics [43, 44]. Statistically significant support for the existence of population cycles among mammals is predominantly based on time series for small mammals [45], where our model would predict more pronounced transient dynamics, given how close these points are to the Hopf bifurcation. On the other hand, the longer gestational times and the increased difficulty in measurements, precludes obtaining similar-quality data for larger organisms.

Extinction risk

Within our model, higher rates of starvation result in a larger flux of the population to the hungry state. In this state reproduction is absent, thus increasing the likelihood of extinction. However, from the perspective of population survival, it is the rate of starvation relative to the rate of recovery that determines the long-term dynamics of the system (Fig. 3). We now examine the competing effects of cyclic dynamics vs. changes in steady state density on extinction risk as a function of the ratio σ/ρ . To this end, we computed the probability of extinction, where extinction is defined as the population trajectory falling below $0.2 \times$ the allometrically constrained steady state for all times between 10^6 and $\leq 10^8$. This procedure is repeated for 1000 replicates of the continuous-time system shown in Eq. 1 for an organism of $M = 100$ grams. In each replicate the initial densities are chosen to be $A(F^*, H^*, R^*)$, with A a random variable that is uniformly distributed in $[0, 2]$. By allowing the rate of starvation to vary, we assessed extinction risk across a range of values of the ratio σ/ρ varying between ca. 10^{-3} to

5, thus examining a horizontal cross-section of Fig. 3. As expected, higher rates of extinction correlated with both low and high values of σ/ρ . For low values of σ/ρ , the increased extinction risk results from transient cycles with larger amplitudes as the system nears the Hopf bifurcation (Fig. 5). For large values of σ/ρ , higher extinction risk arises because of the decrease in the steady state consumer population density. This interplay creates an ‘extinction refuge’ as shown in Fig. 5, such that for a relatively constrained range of σ/ρ , extinction probabilities are minimized.

We find that the allometrically constrained values of σ/ρ (with 20% variability around energetic parameter means) fall within the extinction refuge. These values are close enough to the Hopf bifurcation to avoid low steady state densities, and far enough away to avoid large-amplitude transient cycles. The fact that allometric values of σ and ρ fall within this small window supports the possibility that a selective mechanism has constrained the physiological conditions that drive starvation and recovery rates within populations. Such a mechanism would select for organism physiology that generates appropriate σ and ρ values that avoid extinction. This selection could occur via the tuning of body fat percentages, metabolic rates, and biomass maintenance efficiencies. To summarize, our finding that the allometrically-determined parameters fall within this low extinction probability region suggests that the NSM dynamics may both drive—and constrain—natural animal populations.

Dynamic and energetic barriers to body size

Metabolite transport constraints are widely thought to place strict boundaries on biological scaling [46, 47, 31] and thereby lead to specific predictions on the minimum possible body size for organisms [48]. Above this bound, a number of energetic and evolutionary mechanisms have been explored to assess the costs and benefits associated with larger body masses, particularly for mammals. One important such example is the *fasting endurance hypothesis*, which contends that larger body size, with consequent lower metabolic rates and increased ability to maintain more endogenous energetic reserves, may buffer organisms against environmental fluctuations in resource availability [49].

Over evolutionary time, terrestrial mammalian lineages show a significant trend towards larger body size (known as Cope’s Rule) [50, 51, 52, 53], and it is thought that within-lineage drivers generate selection towards an optimal upper bound of roughly 10^7 grams [50], the value of which may arise from higher extinction risk for large taxa over evolutionary timescales [51]. These trends are thought to be driven by a combination of climate change and niche availability [53]; however the underlying energetic costs and benefits of larger body sizes, and how they influence dynamics over ecological timescales, have not been explored. We argue that the NSM provides a suitable framework to explore these issues.

The NSM correctly predicts that species with smaller masses have larger steady-state population densities (Fig. 6a). However we observe that there is a sharp change in the mass dependence of both the steady-state densities and σ/ρ at $M \approx 0.3$ grams (Fig. 6b,c). The dependence of the rates of starvation and recovery explain this phenomenon. As the mass decreases, the rate of starvation increases, while the rate of recovery decreases super-exponentially. This decline in ρ occurs when the percentage of body fat is $1 - (a/b)^{-1/(\eta-1)} M^{-1} \approx 2\%$, whereupon consumers are unable to recover from the hungry state. Compellingly, this dynamic bound determined by the rate of energetic recovery is close to the minimum observed mammalian body size of ca. 1.3-2.5 grams (Fig. 6b,c), a range that occurs as the recovery rate begins its decline. In addition to known transport limitations [48], we suggest that an additional constraint

of lower body size stems from the dynamics of starvation. This result mirrors other efforts where coincident limitations seem to constrain the smallest possibilities for life within a particular class of organisms [3].

A theoretical upper bound on mammalian body size is given by the decrease in the mass of a blue whale. We determine a more realistic upper bound to body mass by assessing the susceptibility of an otherwise homogeneous population to invasion by a mutated subset of the population (denoted by $'$) where individuals have a modified proportion of body fat $M' = M(1 + \chi)$ where $\chi \in [-0.5, 0.5]$, thus altering the rates of starvation σ , recovery ρ , and maintenance β . There is no internal fixed point that correspond to a state where both original residents and invaders coexist (except for the trivial state $\chi = 0$). To assess the susceptibility to invasion as a function of the invader mass, we determine which consumer has a higher steady-state density for a given value of χ . We find that for $1 \leq M < 10^6$ g, having additional body fat ($\chi > 0$) results in a higher steady-state invader population density ($H'^* + F'^* > H^* + F^*$). Thus the invader has an intrinsic advantage over the resident population.

However, for $M > 10^6$ g, leaner individuals ($\chi < 0$) have the advantage, and this is due to the changing covariance between energetic rates as a function of modified energetic reserves [I don’t understand the phrase after the comma].

The observed switch in susceptibility as a function of χ at $M_{opt} \approx 10^6$ g thus serves as an attractor, where over evolutionary times the NSM predicts organismal mass to increase if $M < M_{opt}$ and decrease if $M > M_{opt}$. Moreover, M_{opt} , which is entirely determined by the population-level consequences of energetic constraints, is within an order of magnitude of the mass observed in the North American mammalian fossil record [50] and also the mass predicted from an evolutionary model of body size evolution [51]. While the state of the environment, as well as the competitive landscape, will determine whether specific body sizes are selected for or against [53], we suggest that the starvation dynamics proposed here may provide the driving mechanism for the evolution of larger body size among terrestrial mammals.

A potential critique of our results, which show that larger mammals are less susceptible to extinction, is why we don’t observe a greater number of large mammals in the modern world. However, recent research suggests that the pleistocene may have been much more populated with a significant diversity of very large mammals [54, 55, 56] which were also much more geographically widespread than today. These results combined with our findings suggest that the modern diversity of mammals may not represent a true steady state the current distribution of nutrients and large seeds may be very different from the past.

The energetics associated with somatic maintenance, growth, and reproduction are important elements that influence the dynamics of all populations [9]. The NSM is a minimal and general model that incorporates the dynamics of starvation that are expected to occur in resource-limited environments. By incorporating allometric relations between the rates in the NSM, we find: (i) different organismal masses have distinct population dynamic regimes, (ii) allometrically-determined rates of starvation and recovery appear to minimize extinction risk, and (iii) the dynamic consequences of these rates may place additional barriers on the evolution of minimum and maximum body size. We suggest that the NSM offers a means by which the dynamic consequences of energetic constraints can be assessed using macroscale interactions between and among species. Future efforts will involve exploring the consequences of these dynamics in a spatially explicit framework, thus incorporating elements

475 such as movement costs and spatial heterogeneity, which may 476 elucidate additional tradeoffs associated with the dynamics of
477 starvation.

- 478 1. Martin TE (1987) Food as a Limit on Breeding Birds: A Life-History Perspective. *Annu. Rev. Ecol. Syst.* 18:453–487.
479 2. Kirk KL (1997) Life-History Responses to Variable Environments: Starvation and
480 Reproduction in Planktonic Rotifers. *Ecology* 78:434–441.
481 3. Kempes CP, Dutkiewicz S, Follows MJ (2012) Growth, metabolic partitioning, and
482 the size of microorganisms. *PNAS* 109:495–500.
483 4. Mangel M, Clark CW (1988) *Dynamic Modeling in Behavioral Ecology* (Princeton
484 University Press, Princeton).
485 5. Morris DW (1987) Optimal Allocation of Parental Investment. *Oikos* 49:332.
486 6. Tveraa T, Fauchald P, Henaug C, Yoccoz NG (2003) An examination of a com-
487 pensatory relationship between food limitation and predation in semi-domestic
488 reindeer. *Oecologia* 137:370–376.
489 7. Daan S, Dijkstra C, Drent R, Meijer T (1988) *Food supply and the annual timing of
490 avian reproduction*.
491 8. Jacot A, Valcu M, van Oers K, Kempenaers B (2009) Experimental nest site lim-
492 itation affects reproductive strategies and parental investment in a hole-nesting
493 passerine. *Animal Behaviour* 77:1075–1083.
494 9. Stearns SC (1989) Trade-Offs in Life-History Evolution. *Funct. Ecol.* 3:259.
495 10. Barboza P, Jorda D (2002) Intermittent fasting during winter and spring affects body
496 composition and reproduction of a migratory duck. *J Comp Physiol B* 172:419–434.
497 11. Threlkeld ST (1976) Starvation and the size structure of zooplankton communities.
498 *Freshwater Biol.* 6:489–496.
499 12. Weber TP, Ens BJ, Houston AI (1998) Optimal avian migration: A dynamic model
500 of fuel stores and site use. *Evolutionary Ecology* 12:377–401.
501 13. Mduma SAR, Sinclair ARE, Hilborn R (1999) Food regulates the Serengeti wilde-
502 beest: a 40-year record. *J. Anim. Ecol.* 68:1101–1122.
503 14. Moore JW, Yeakel JD, Peard D, Lough J, Beere M (2014) Life-history diversity and its
504 importance to population stability and persistence of a migratory fish: steelhead
505 in two large North American watersheds. *J. Anim. Ecol.* 83:1035–1046.
506 15. Mead RA (1989) in *Carnivore Behavior, Ecology, and Evolution* (Springer US,
507 Boston, MA), pp 437–464.
508 16. Sandell M (1990) The Evolution of Seasonal Delayed Implantation. *The Quarterly
509 Review of Biology* 65:23–42.
510 17. Bulik CM, et al. (1999) Fertility and Reproduction in Women With Anorexia Nervosa.
511 *J. Clin. Psychiatry* 60:130–135.
512 18. Trites AW, Donnelly CP (2003) The decline of Steller sea lions *Eumetopias jubatus*
513 in Alaska: a review of the nutritional stress hypothesis. *Mammal Review* 33:3–28.
514 19. Glazier DS (2009) Metabolic level and size scaling of rates of respiration and growth
515 in unicellular organisms. *Funct. Ecol.* 23:963–968.
516 20. Kooijman SALM (2000) *Dynamic Energy and Mass Budgets in Biological Systems*
517 (Cambridge).
518 21. Sousa T, Domingos T, Poggiale JC, Kooijman SALM (2010) Dynamic energy budget
519 theory restores coherence in biology. *Philos. T. Roy. Soc. B* 365:3413–3428.
520 22. Diekmann O, Metz JAJ (2010) How to lift a model for individual behaviour to the
521 population level? *Philos. T. Roy. Soc. B* 365:3523–3530.
522 23. Murdoch WW, Briggs CJ, Nisbet RM (2003) *Consumer-resource Dynamics*, Mono-
523 graphs in population biology (Princeton University Press).
524 24. Guckenheimer J, Holmes P (1983) *Nonlinear oscillations, dynamical systems, and
525 bifurcations of vector fields* (Springer, New York).
526 25. Gross T, Feudel U (2004) Analytical search for bifurcation surfaces in parameter
527 space. *Physica D* 195:292–302.
528 26. Hastings A (2001) Transient dynamics and persistence of ecological systems. *Ecol. Lett.* 4:215–220.
529 27. Neubert M, Caswell H (1997) Alternatives to resilience for measuring the responses
530 of ecological systems to perturbations. *Ecology* 78:653–665.
531 28. Caswell H, Neubert MG (2005) Reactivity and transient dynamics of discrete-time
532 ecological systems. *Journal of Difference Equations and Applications* 11:295–310.
533 29. Neubert M, Caswell H (2009) Detecting reactivity. *Ecology*.
534 30. Yodzis P, Innes S (1992) Body Size and Consumer-Resource Dynamics. *Am. Nat.*
535 139:1151–1175.
536 31. Brown J, Gillooly J, Allen A, Savage V, West G (2004) Toward a metabolic theory of
537 ecology. *Ecology* 85:1771–1789.
538 32. West GB, Woodruff WH, Brown JH (2002) Allometric scaling of metabolic rate from
539 molecules and mitochondria to cells and mammals. *Proc. Natl. Acad. Sci. USA* 99:
540 Suppl 1:2473–2478.
541 33. DeLong JP, Okie JG, Moses ME, Sibly RM, Brown JH (2010) Shifts in metabolic
542 scaling, production, and efficiency across major evolutionary transitions of life.
543 *PNAS* 107:12941–12945.
544 34. West GB, Brown JH, Enquist BJ (2001) A general model for ontogenetic growth.
545 *Nature* 413:628–631.
546 35. Moses ME, et al. (2008) Revisiting a Model of Ontogenetic Growth: Estimating Model
547 Parameters from Theory and Data. <http://dx.doi.org.proxy.lib.sfu.ca/10.1086/679735>
548 171:632–645.
549 36. Gillooly JF, Charnov EL, West GB, Savage VM, Brown JH (2002) Effects of size and
550 temperature on developmental time. *Nature* 417:70–73.
551 37. Hou C, et al. (2008) Energy Uptake and Allocation During Ontogeny. *Science*
552 322:736–739.
553 38. Folland JP, Mc Cauley TM, Williams AG (2008) Allometric scaling of strength mea-
554 surements to body size. *Eur J Appl Physiol* 102:739–745.
555 39. Calder III WA (1983) An allometric approach to population cycles of mammals. *J.
556 Theor. Biol.* 100:275–282.
557 40. Peterson RO, PAGE RE, DODGE KM (1984) Wolves, Moose, and the Allometry of
558 Population Cycles. *Science* 224:1350–1352.
559 41. Krukonis G, Schaffer WM (1991) Population cycles in mammals and birds: Does
560 periodicity scale with body size? *J. Theor. Biol.* 148:469–493.
561 42. Hendriks AJ, Mulder C (2012) Delayed logistic and Rosenzweig(MacArthur models
562 with allometric parameter setting estimate population cycles at lower trophic levels
563 well. *Ecological Complexity* 9:43–54.
564 43. Kendall BE, et al. (1999) Why do populations cycle? A synthesis of statistical and
565 mechanistic modeling approaches. *Ecology* 80:1789–1805.
566 44. Höglstedt G, Seldal T, Breistol A (2005) Period length in cyclic animal populations.
567 *Ecology* 86:373–378.
568 45. Kendall, Prendergast, Bjørnstad (1998) The macroecology of population dynamics:
569 taxonomic and biogeographic patterns in population cycles. *Ecol. Lett.* 1:160–164.
570 46. Brown J, Marquet P, Taper M (1993) Evolution of body size: consequences of an
571 energetic definition of fitness. *Am. Nat.* 142:573–584.
572 47. West GB, Brown JH, Enquist BJ (1997) A General Model for the Origin of Allometric
573 Scaling Laws in Biology. *Science* 276:122–126.
574 48. West GB, Woodruff WH, Brown JH (2002) Allometric scaling of metabolic rate from
575 molecules and mitochondria to cells and mammals. *Proc. Natl. Acad. Sci. USA*
576 99:2473–2478.
577 49. Millar J, Hickling G (1990) Fasting Endurance and the Evolution of Mammalian
578 Body Size. *Funct. Ecol.* 4:5–12.
579 50. Alroy J (1998) Cope's rule and the dynamics of body mass evolution in North
580 American fossil mammals. *Science* 280:731.
581 51. Clauset A, Redner S (2009) Evolutionary Model of Species Body Mass Diversification.
582 *Phys. Rev. Lett.* 102:038103.
583 52. Smith F, Boyer A, Brown J, Costa D (2010) The Evolution of Maximum Body Size of
584 Terrestrial Mammals. *Science*.
585 53. Saarinen JJ, et al. (2014) Patterns of maximum body size evolution in Cenozoic
586 land mammals: eco-evolutionary processes and abiotic forcing. *Proc Biol Sci*
587 281:20132049–20132049.
588 54. Doughty CE, Wolf A, Malhi Y (2013) The legacy of the Pleistocene megafauna
589 extinctions on nutrient availability in Amazonia. *Nature Geosci* 6:761–764.
590 55. Doughty CE, et al. (2016) Megafauna extinction, tree species range reduction, and
591 carbon storage in Amazonian forests. *Ecography* 39:194–203.
592 56. Doughty CE, Faurby S, Svenning JC (2016) The impact of the megafauna extinctions
593 on savanna woody cover in South America. *Ecography* 39:213–222.
594 595 596 **ACKNOWLEDGMENTS.** We thank Luis Bettancourt, Eric Libby, Seth Newsome,
597 et al. for helpful discussions and comments that greatly increased the quality of
598 the manuscript. J.D.Y. was supported by startup funds at the University of Califor-
599 nia, Merced, and an Omidyar postdoctoral Fellowship at the Santa Fe Institute.
600 C.P.K. was supported by an Omidyar postdoctoral Fellowship at the Santa Fe
601 Institute. S.R. was supported by grants DMR-1608211 and 1623243 from the
602 National Science Foundation, and by the John Templeton Foundation, all at the
603 Santa Fe Institute.

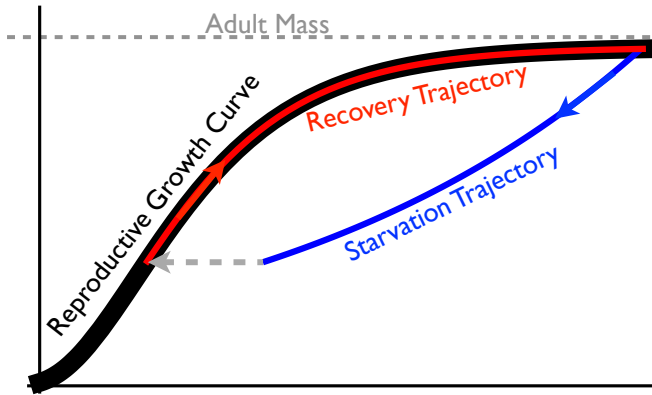


Fig. 1: The growth trajectory over absolute time of an individual organism as a function of body mass. Initial growth follows the red trajectory to an energetically replete adult mass M . Starvation follows the concave blue trajectory to $m_{\text{starve}} < M$, whereas recovery follows the convex growth trajectory from m_σ to M .

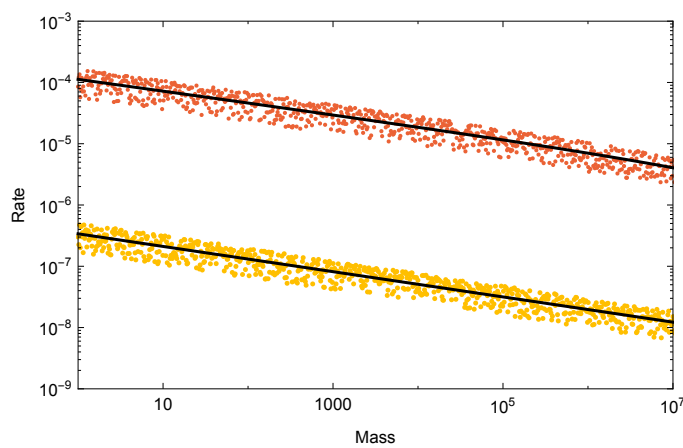


Fig. 2: Allometrically constrained starvation rate σ (red) vs. reproductive rate λ (yellow) as a function of mass M . The rate of starvation is greater than the rate of reproduction for all realized terrestrial endotherm body sizes.

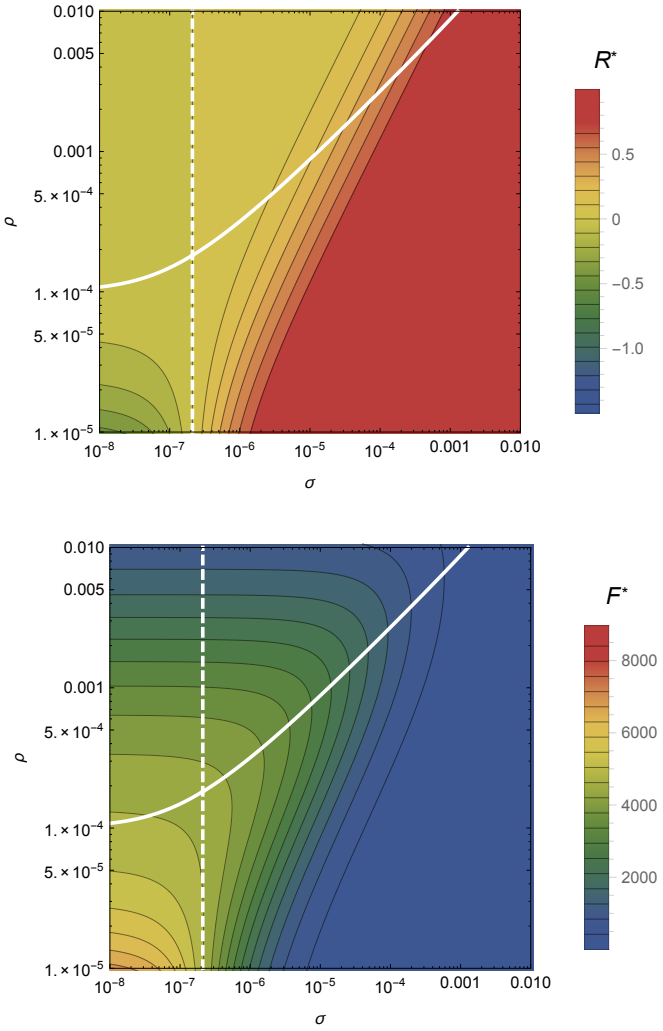


Fig. 3: The transcritical (TC; dashed line) and Hopf bifurcation (solid line) as a function of the starvation rate σ and recovery rate ρ . These bifurcation conditions separate parameter space into infeasible, cyclic, and steady state dynamic regimes. The color gradient shows the steady state densities for (A) the resource R^* and the (B) energetically replete consumers F^* , with warm colors denoting higher densities and cool colors denoting lower densities. Steady state densities for the energetically deficient consumers H^* are not shown because they closely mirror those for F^* .

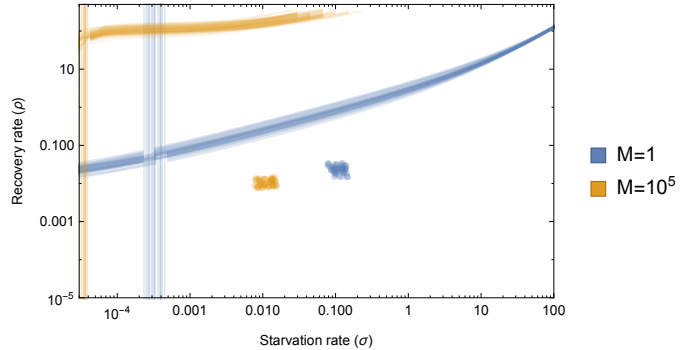


Fig. 4: Transcritical (TC; vertical lines) and Hopf bifurcations (curved lines) with allometrically determined starvation σ and recovery ρ rates as a function of minimum and maximum mammalian body sizes: 1 gram (blue) and 10^7 grams (orange), respectively. Replicates show the influence of variation (20% around the mean) on allometric parameters, which influences both the energetic rates as well as the position of the TC and Hopf bifurcations.

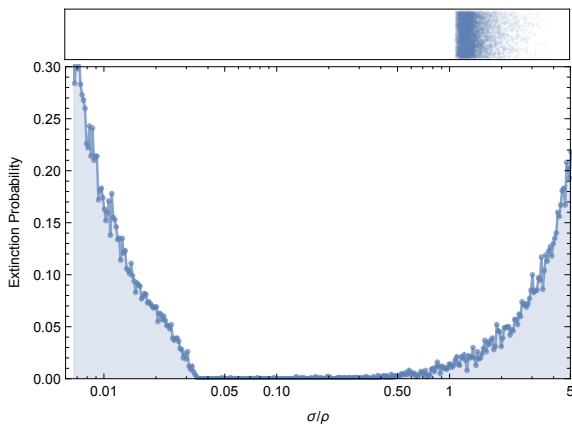


Fig. 5: The probability of extinction for 1000 consumer population trajectories as a function of σ/ρ within initial densities chosen to as $A(F^*, H^*, R^*)$, with A a random variable that is uniformly distribution in $[0, 2]$. Extinction is defined as the population trajectory going below $0.2 \times$ the allometrically constrained steady state for all times between 10^2 and $\leq 10^6$. The values above the extinction plot are the allometrically constrained σ/ρ with 20% variation around the mean.

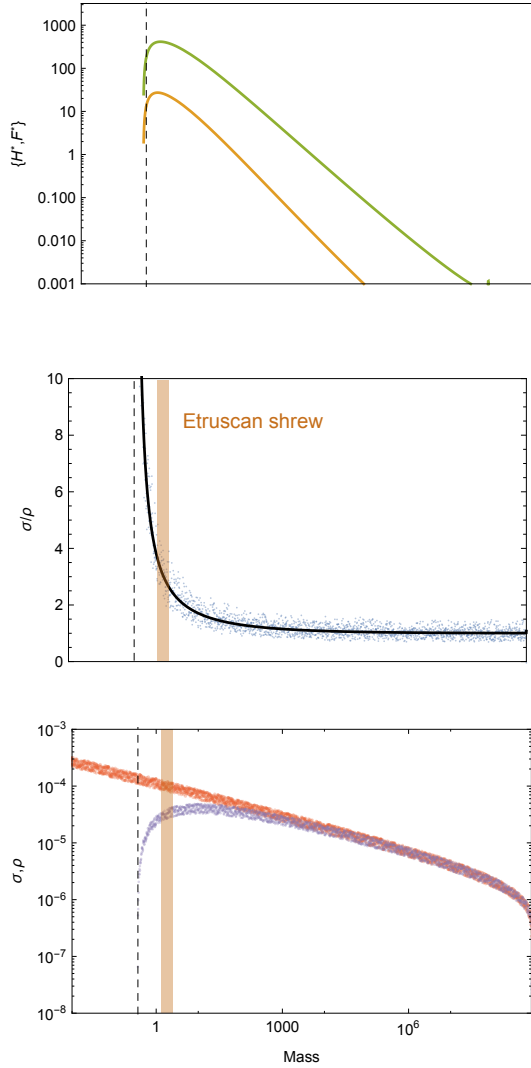


Fig. 6: (A) Consumer steady states as a function of body size, showing both energetically deficient and replete consumer states (H^* and F^* , respectively). Energetic rates as a function of body size, with the ratio σ/ρ (B) and both σ (red) and ρ (purple; C) drawn separately with 20% variation around the mean. Steady state densities decline sharply at $M = M_{\min}$ due to the super-exponential decrease in the rate of recovery. The minimum body size observed for mammals (the Etruscan shrew) is denoted by the orange shaded region at values marking the initial decline of the recovery rate.

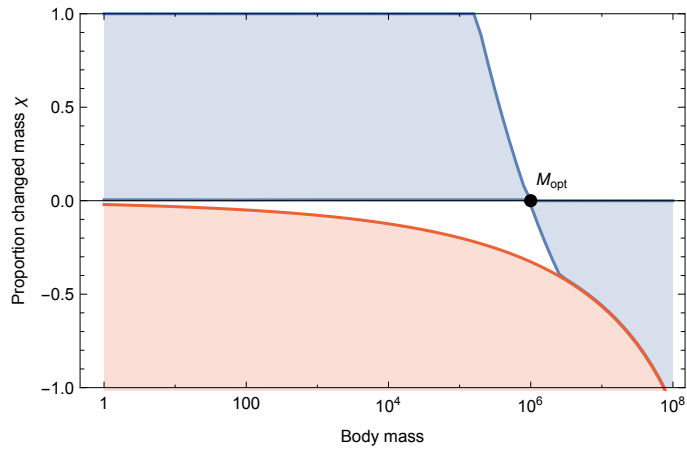


Fig. 7: Invasion feasibility for organisms with a proportional change in mass χ against a population with a resident body mass M . The blue region denotes which values of χ result in successful invasion. The red region denotes which values of χ result in a mass that is below the starvation threshold and is thus infeasible.